A Morphing Radiator for High-Turndown Thermal Control of Crewed Space Exploration Vehicles

Thomas J. Cognata[1]
Business or Academic Affiliation 1, City, State, Zip Code

Darren Hardtl[2]
Business or Academic Affiliation 2, City, Province, Zip Code, Country

and

Rubik Sheth[3], Craig Dinsmore[4]
Business or Academic Affiliation 3, City, State, Zip Code

Spacecraft designed for missions beyond low earth orbit (LEO) face a difficult thermal control challenge, particularly in the case of crewed vehicles where the thermal control system (TCS) must maintain a relatively constant internal environment temperature despite a vastly varying external thermal environment and despite heat rejection needs that are contrary to the potential of the environment. A thermal control system is in other words required to reject a higher heat load to warm environments and a lower heat load to cold environments, necessitating a quite high turndown ratio. A modern thermal control system is capable of a turndown ratio of on the order of 12:1, but for crew safety and environment compatibility these are massive multi-loop fluid systems. This paper discusses the analysis of a unique radiator design which employs the behavior of shape memory alloys (SMA) to vary the turndown of, and thus enable, a single-loop vehicle thermal control system for space exploration vehicles. This design, a morphing radiator, varies its shape in response to facesheet temperature to control view of space and primary surface emissivity. Because temperature dependence is inherent to SMA behavior, the design requires no accommodation for control, instrumentation, nor power supply in order to operate. Thermal and radiation modeling of the morphing radiator predict a turndown ranging from 11.9:1 to 35:1 independent of TCS configuration. Stress and deformation analyses predict the desired morphing behavior of the concept. A system level mass analysis shows that by enabling a single loop architecture this design could reduce the TCS mass by between 139 kg and 225 kg. The concept is demonstrated in proof-of-concept benchtop tests.

[1] Insert Job Title, Department Name, Address/Mail Stop, and AIAA Member Grade for first author.
[2] Insert Job Title, Department Name, Address/Mail Stop, and AIAA Member Grade for third author.
[3] Insert Job Title, Department Name, Address/Mail Stop, and AIAA Member Grade for fourth author (etc).
[4] Insert Job Title, Department Name, Address/Mail Stop, and AIAA Member Grade for fourth author (etc).

I. Introduction

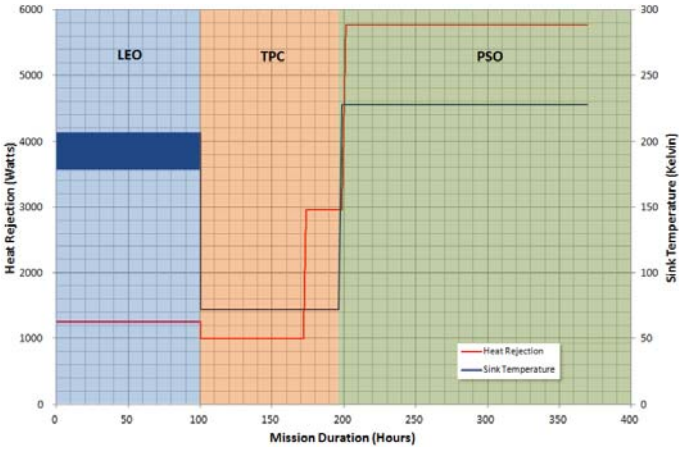

Figure 1 A representative mission profile illustrating varying thermal environment and heat rejection.

Spacecraft designed for missions beyond low earth orbit (LEO) face a difficult thermal control challenge, particularly in the case of crewed vehicles. The thermal control system must maintain a relatively constant internal environment temperature despite a vastly varying external thermal environment. The external environment may present a sink temperature that ranges from 70 K in trans-planetary coast (TPC) to approximately 228K in planetary surface operations (PSO), and heat rejection needs that are contrary to the change in capacity of the environment. In other words, the thermal control system (TCS) is required to reject a higher heat load to warm environments and a lower heat load to cold environments, necessitating a quite high turndown ratio.

This thermal design need is complicated by the challenge of transporting heat from crewed portions of the vehicle to the heat rejection portion of a TCS without the endangerment of crewmembers by working fluid toxicity or by potential reaction of the working fluid with other vehicle systems due to a leak. This drives the current state of the art TCS design – a two-loop system with a propylene-glycol/water working fluid contained in an inner TCS loop and with a low freezing point refrigerant in a loop wholly external to the cabin which is able to operate over the very wide range of temperatures that the radiator is subject to. This design has the drawback of adding significant mass and complexity to the TCS, interfacial inefficiencies to heat transfer between the loops, and the duplication of fluid handling equipment such as pumps and expansion tanks. Previous trades [19,20] have shown that a two-loop TCS may be approximately 25% heavier than a similarly performing single loop system.

This work describes a unique louvre-derivative radiator which employs the shape memory behavior of Nitinol to produce very high turn-downs ratios capable of enabling single-loop thermal control of a vehicle using propylene-glycol or similar common, non-toxic, high freezing-point working fluids.

II. The Morphing Radiator

This technology employs the shape memory effect in conjunction with an integral bias load to actuate the surface of a radiator. The basic function of this concept is illustrated in Figure 7. The radiator takes one of two basic shapes depending on the temperature of the facesheet. When hot the radiator will take its fully extended austenitic shape, shown at the top of the figure. When cold the radiator takes its deformed martensitic shape, the semi-circle shown in the bottom of the figure. By varying shape this concept alters the view factor of the radiator to space, maximizing view in the hot case and minimizing it in the cold case. The thermal effect of this geometric actuation is multiplied by selective surface emissivity, where the top surface has a high emissivity and the bottom surface a low emissivity.

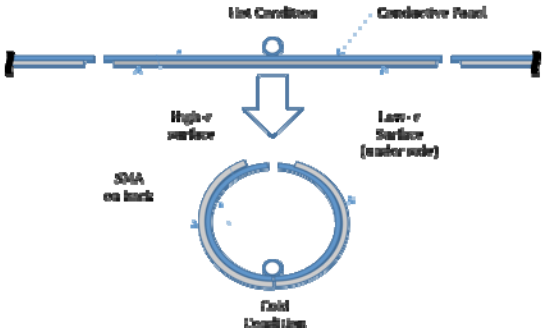

Figure 3 A conceptual illustration of the technology. *Top shows the austenitc shape at high temperature and below is the deformed martensitic shape at low temperature. A central tube carries a thermal working fluid.*

An illustration of an array of such panels is shown in Figure 6. This demonstrates the proportional turndown response of this concept in a parallel flow radiator configuration. Hot fluid enters the inlet header to this array at the top left of the figure from which it enters each flow tube. Working fluid temperature, and thus radiator panel temperature, decreases along the length of each flow tube as heat is rejected through radiation.

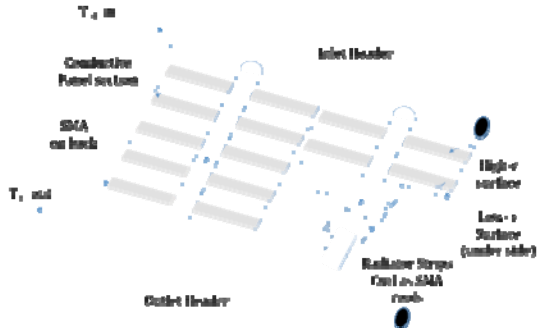

Figure 2 An illustration of an array of panels in a parallel flow radiator configuration. *The array illustrates the passive proportional turn-down of such a system design; as heat is rejected and the working fluid cools, downstream panels take the cold shape and limit the heat rate. The result is a thermal control system which is responsive to the heat rejection needs of the vehicle.*

In a hot environment, as illustrated by the left most flow tube and panels in Figure 6, the working fluid and panel temperature remains above the shape memory transition temperature so all panels are in the hot state. Thus, heat is rejected through the greatest possible radiator area. In a cool environment, however, represented by the right most flow tube and panels in Figure 6, panels begin taking the cold shape and limiting heat rejection toward the end of the flow tube as the working fluid temperature falls below the transition temperature of the shape memory alloy. As a result of such behavior this radiator design will tend to maintain a minimum system fluid temperature in the vicinity of the M_f temperature of the shape memory alloy, a behavior that can vastly simplify control design of the thermal control system for a vehicle. The target control temperature for a single

loop thermal control system using a PGW working fluid is in the vicinity of -10°C, an ideal fit for medical grade nitinol.

This technology may be integrated into a single loop thermal control system in place of the traditional radiator shown in Figure 9. No accommodation is needed for control, power source, or instrumentation as the actuation of this technology is passive and a function of the inherent temperature dependence of the shape memory material.

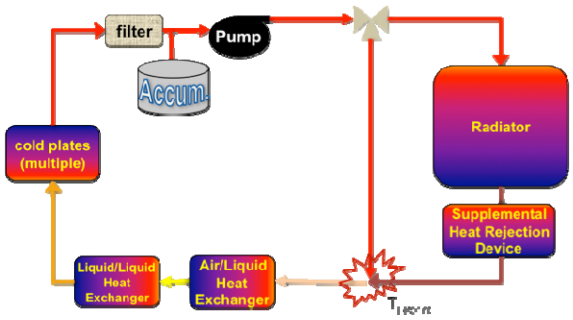

Figure 4 Concept A Thermal control system design. *A single loop thermal control system integrating Concept A as the Radiator.*

III. Turn-down and Thermal Analysis

A first order evaluation of performance of this concept is found through the definition of radiation heat rejection,

$$Q_i = F_i \cdot \varepsilon_i \cdot \sigma \cdot A \cdot \left(T_{surface}^4 - T_{space}^4\right),$$

where Q_i is the heat rate, F_i is the view factor of the radiator, ε_i the emissivity of the active area, σ the Stephan-Boltzmann constant, A the total radiator surface area, $T_{surface}$ the temperature of the radiator surface, and T_{space} the sink temperature. The concept turndown in this ideal case is a ratio of the high and low states, or

$$R = \frac{\left(\sum F_{i,space} \cdot \varepsilon_i\right)\left(T_{surface}^4 - T_{\sin k}^4\right)_{Hot}}{\left(\sum F_{i,space} \cdot \varepsilon_i\right)\left(T_{surface}^4 - T_{\sin k}^4\right)_{Cold}}$$

where the subscript *i* refers to a surface, e.g. top and bottom, the subscript *Hot* reflects values of the high heat rejection shape and hot environment and the subscript *Cold* reflects values of the low heat rejection shape and cold environment.

Table 1 Defining characteristics.

	Hot	Cold
$F_{top,space}$	1	0.031
ε_{top}	0.81	
$F_{bottom,space}$	<0.001	0.560
ε_{bottom}	0.015	
T_{sink}	230 K	70 K
$T_{surface}$	293 K	
Radius	r	
Length	32 r	
Width	2π r	

This concept is capable of a 15:1 turndown based on the parameters and the environments described in Figure 1 and Table 1. Table 1 shows the view factor and emissivity for each surface in both hot and cold cases. Emissivity of the top surface is typical of a silver Teflon coating. [23] Emissivity of the bottom surface is typical of highly polished metal or of MLI blankets for medium area applications. [24] The top surface view factor in the cold case is calculated as that of the inner surface of a cylinder through its open ends. [25] Bottom surface view factors assume the radiator to be body mounted to a vehicle. [26, 27].

A turndown of 60:1 becomes possible with shields located at each end of the cylinder formed by the cold shape as these drive the cold value of $F_{top,space}$ toward zero. This range of turndown greatly exceeds the current state of the art and indicates the design room available to meet mission based turn-down needs where conditions do not match analytical assumptions. In fact, it is useful to note that the turndown ratio is a product of two turn-down terms, the physical turn-down which is composed of the view factor and emissivity and a consequence of design, and the environmental turn-down which is described by temperatures. The physical turn-down is 96:1 with end shields, 25:1 without.

A finite difference representation was created using Thermal Desktop with FLUINT in order to predict the concept turndown with higher fidelity and with a simulated fluid loop. The representation includes a parameterized radiator geometry, a simplified thermal control fluid loop, and simplified geometry representing a vehicle.

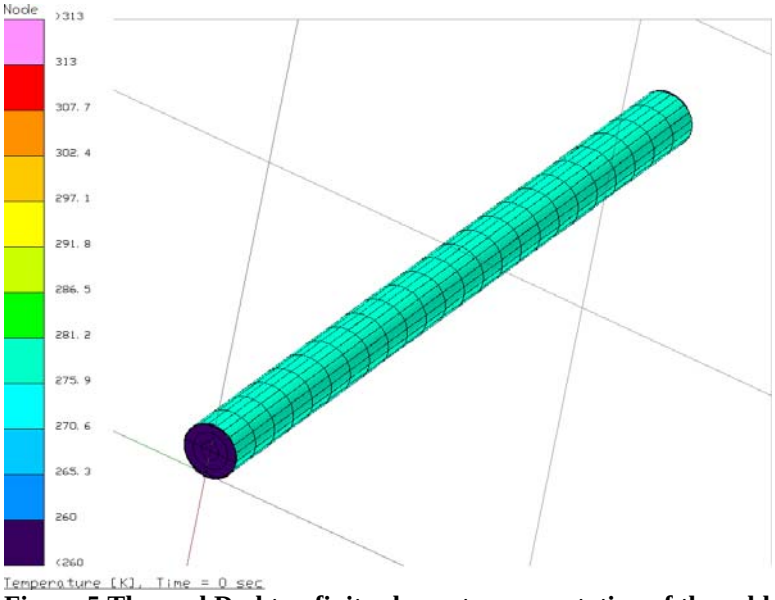

Figure 5 Thermal Desktop finite element representation of the cold shape. *The model is parametric: this shows geometry given the minimum radius.*

Figure 10 and Figure 11 show the cold and hot case analysis geometries, respectively. These figures show the radiator and fluid path; the vehicle geometry and the balance of the thermal control loop is hidden for clarity. The model is built using Thermal Desktop native geometry, as opposed to finite element geometric approximations, so that calculations are

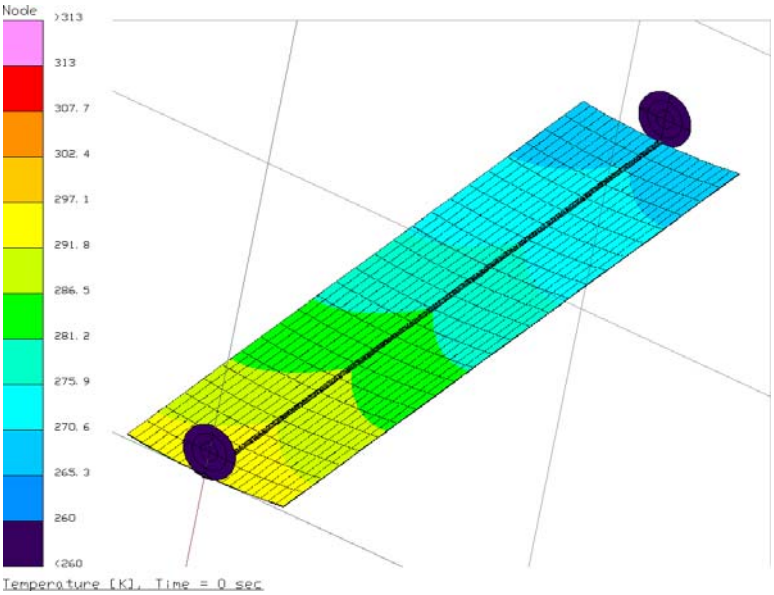

Figure 6 Thermal Desktop finite element representation of the hot shape. *The model is parametric: this shows geometry given the maximum radius.*

mathematically accurate. [28] Thermal Desktop employs a Monte Carlo ray tracing method to calculate the view factor of each element of the geometry for high confidence radiation heat transfer prediction.

The working fluid in the fluid loop is a 50/50 ratio of propylene glycol to water and is based on a property deck which includes experimentally measured data at low temperatures approaching the fluid's glassy state. A set of design optimization studies are performed to determine total area extent of the radiator, panel width (or tube spacing), and panel length that meet the representative mission needs described by Figure 1. Table 3 outlines the key inputs and selected performance parameters that define the model. The system flow rate is set to provide a radiator inlet temperature of 40°C given a system setpoint temperature of 1.7°C. These system temperatures are selected based on the ranges employed in previous vehicle studies including several of Orion [1], Altair [2], and MMSEV [30,31]. The fluid model uses path duplication to apportion the applied vehicle heat load and flow rate to the single panel geometry as if it were one in an array of parallel panels.

Table 3 Thermal modeling parameters.

Parameter	Hot	Cold
Fluid T_{in}	40°C	8.1°C
Q_{load}	5.8 kW	≤1 kW
Total Area	34.8 m^2	
Panel width	24 cm	
Panel Length	1.2 m	
Segment length	10 cm	
$\dot{m}$	175 kg/h	
c_p (@ 10°C)	3354 J/kg-K	
n_{panels}	121	
$T_{setpoint}$	1.7°C	
$kA_{panel,x\ (unit\ length)}$	≥0.152 W-m/K	

Table 2 Composite facesheet properties

Thickness	0.64 mm
k_x panel	360 W/m-K
$k_{y,z}$ panel	0.21 W/m-K
$kA_{panel,x}$	0.230 W-m/K
$\rho_{facesheet}$	1875 kg/m^3
ρ''_{panel}	2.49 kg/m^2

IV. Stress and Deformation Analysis

With regard to the shape memory alloy constitutive model, we require one that captures all the pertinent thermal and mechanical effects of interest. This includes in particular the martensitic transformation initiated and maintained by some combination of stress and temperature and the effects of heat transfer. To this end, we have chosen the model from the legacy work of Lagoudas, Hartl, and coworkers [34]. It is phenomenological in its formulation and calibration and considers the average thermo-mechanical response of a given representative volume element (RVE) by first postulating RVE-averaged energy and dissipation potentials. This thermodynamically oriented approach allows for straightforward formulation of couplings between the energetics of heat transfer and those of deformation, which are so critical in the analysis of SMAs. Further, we have herein taken the approach of Hartl and Lagoudas [35], which considers the effects of large structural deformations (rotations) as will be common in the current work.

The overall hierarchical analysis tool is flexible and modular; different simulation process managers, FEA tools, or constitutive models can be substituted at any time. In the current work, we utilize a proven combination of the Abaqus Unified FEA Suite and user material subroutines [33]. Abaqus is used to perform preprocessing, processing, and post-processing operations, while the user material subroutine (UMAT) associated with the constitutive model has been coded in Fortran.

The stress and deformation analysis focused on heat transfer from a central rod that simulates the flow pipe and into the attached "winglets" of the concept, which include SMA material regions. The winglets are formed in an initially stress-free cylindrical shape. Sufficient heating of SMA material placed around the outer diameter of the cylinder leads to strain recovery and thus flattening of the winglet, increasing the heat rejection effectiveness of the structure as a radiator. The capabilities of the SMA to affect this behavior and the capability of the elastic composite laminate to withstand it without failure will be assessed in this analysis.

The finite element model for this concept considers the coupled thermal and mechanical responses of all bodies involved. In such analysis, localized and evolving thermal conditions resulting from the physics of heat transfer drive the local transformation-induced deformation response in the SMA, which then leads to deformation in other material regions depending on imposed mechanical coupling constraints (i.e., contact or mesh ties). The model considered two key structural components: the flow tube and the flexible winglet. The flow tube was modeled as a simple aluminum tube for reasons to be described, while the winglet itself was modeled as a laminate shell. Two specific design options were considered with regard to the configuration of the active SMA component(s).

- One option considered two bundles of SMA wires tied to the petal edges and in contact with the outer layer of the winglet elsewhere (*SMA Wire option*). The model associated with this design utilized 540 linear 3-D elements (C3D8T) for the flow tube, 825 quadratic shell elements (S8RT) for the composite winglet, and 33 quadratic shell elements (S8RT) for the SMA wire bundles.
- The second considered the use of an SMA thin sheet or foil, which enters the analysis as an additional (thermally active) lamina in the winglet composite layup (*SMA Film option*). Analysis of this design is much more computationally efficient and also highlights the flexibility of the implemented SMA model in directly calculated intra-laminar SMA response, which assumes plane stress conditions. The model associated with this design utilized 540 linear 3-D elements (C3D8T) for the flow tube and 825 quadratic shell elements (S8RT) for the composite winglet that includes an SMA film layer.

Models for both design options assumed lengthwise symmetry with respect to the flow tube for the purposes of computational efficiency. The analysis model for the SMA wire option including a detail of the composite layup is shown in Figure 10. The bottom lamina in the layup as shown corresponds to the inner diameter of the curled winglet. The model for the SMA film design option is very similar. The SMA wire regions are removed and an additional lamina is added to the shell composite layup. This augmented and annotated layup is detailed in Figure 11.

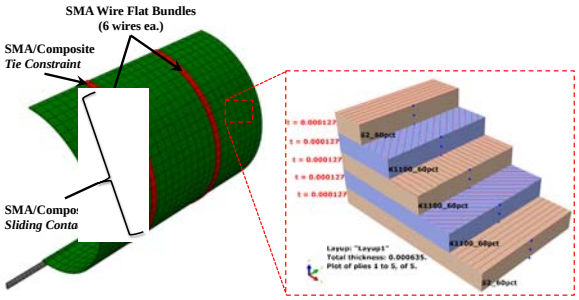

Figure 7 - Coupled thermo-structural finite element model of Concept A (SMA wire option) with composite layup detail.

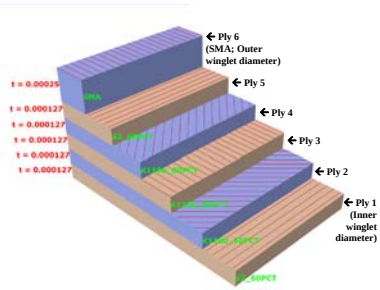

Figure 8 – Winglet composite layup for the coupled thermo-structural finite element model of Concept A (SMA film option)

The time history of thermal conditions used in this analysis reflects the preliminary assumption that the winglet response is driven completely by the *temperature* of the flow tube (i.e., a temperature boundary condition), and that this temperature varies negligibly over the length of a single winglet. Based on this assumption, the current thermally coupled analysis considered a case in which the flow tube temperature was increased in a spatially homogeneous manner from T=263K to T=313K over 60 s followed by a 10 s dwell. Due to this even heating, the tube was modeled as a simple solid aluminum body. The transient propagation of heat outward from the flow tube and into the SMA film layer in the winglets induces the phase transformation, which leads to strain recovery and deformation of the initially cylindrical winglet toward a flat configuration.

The critical material behaviors of interest in this study were associated with both the flexible composite radiator winglets and the SMA wire/film that drives the bending deformation of those winglets. The composite was assumed to be constructed from carbon fiber-based and glass fiber-based unidirectional laminae, and these lamina properties were carefully obtained from micromechanical calculations considering fiber and epoxy matrix properties, themselves obtained from a number of sources including commercial composites software databases (the epoxy) and published manufacturer data (the fibers). K1100 fibers were chosen especially for their high thermal conductivity in the fiber direction. Glass fiber laminae were used to provide structural integrity in the transverse direction. The properties of the carbon fiber and glass fiber laminae are given in Table 7.

Table 4 - Material properties for K1100 carbon fiber-based lamina

Material Property	K-1100 carbon fiber	S2 glass fiber
ρ	1812 kg/m^3	1969 kg/m^3
E_1	557 GPa	54.4 GPa
E_2	6.23 GPa	15.9 GPa
ν_{12}	0.318	0.252
G_{12}	0.451 GPa	5.81 GPa
G_{13}	0.451 GPa	5.81 GPa
G_{23}	0.305 GPa	5.69 GPa
$k_{11}=k_{33}$	594 W/m/K	0.861W/m/K
k_{22}	0.0 W/m/K	0.0 W/m/K
c	1000 J/kg/K	1000 J/kg/K

Determining an appropriate composite layup was a matter of iterative analysis. The thermal team set a *kA* minimum of 0.152 W-m/K, which is met using 0.64 mm thickness and at least two carbon fiber laminae aligned perpendicular to the flow tube. It was determined that a more effective three carbon fiber laminae design could be employed without substantial lamina fiber failure if two such laminae were aligned at 45° angles relative to the flow tube. The final layup for the Concept A analysis considered herein is given as described in Table 8. Note that fiber "Angle" is here given relative to the circumferential direction of the cylindrical winglet (i.e., a 90° is aligned with the flow tube).

The properties of the SMA wire were estimated from the response of commercially available pre-trained material. The transformation temperatures, however, were artificially adjusted to match the range required for operation of the radiator according to the thermal analysis. This reflects the need in later development studies to properly choose and characterize the appropriate SMA alloy system. Note that material with the required temperatures is expected to be widely available due to the prevalence of medical-grade NiTi, which transforms in the required temperature range. The properties used in the current analysis are given in Table 10

Table 5 - Composite layup of flexible radiator winglet as used in the analysis of Concept A (SMA foil option adds a 6th ply).

Ply	Material	Depth (mm)	Angle
1	60% S2 Glass in 5250 Epoxy	0.127	90°
2	60% K1100 in 5250 Epoxy	0.127	45°
3	60% K1100 in 5250 Epoxy	0.127	0°
4	60% K1100 in 5250 Epoxy	0.127	45°
5	60% S2 Glass in 5250 Epoxy	0.127	90°

Table 6 - Material properties of the SMA wire as used in the analysis of Concept A.

Material Property	Value
ρ	6450 kg/m^3
G^A	70 GPa
G^M	30 GPa
M_s, M_f	-14°C, -40°C
A_s, A_f	5°C, 32°C
C^A, C^M	6 MPa/K, 7MPa/K (@ 300 MPa)
H_{max}	3.9%
k	0.013/MPa
n_1, n_2, n_3, n_4	0.5, 0.5, 0.5, 0.5
k	22 W/m/K
c	329 J/kg/K

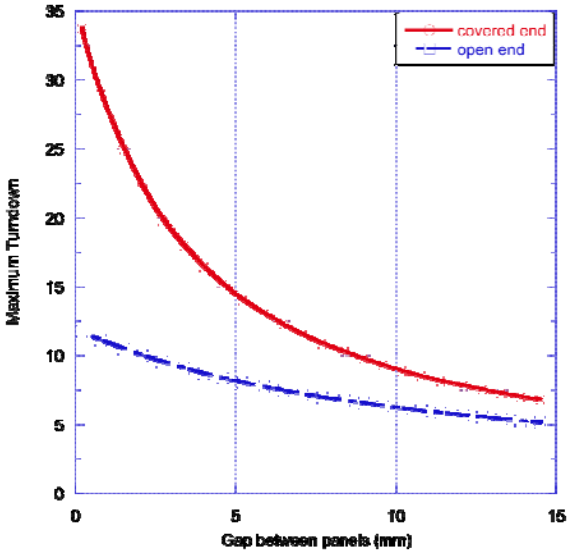

Figure 9 Sensitivity to gap in the cold case. *Shows sensitivity of turndown to the gap between the end of each side of the facesheet for this concept, with and without end shields.*

V. Analysis Results

The thermal model indicates that the concept turndown approaches 11.9 and 35.2 for open end and closed end geometry, where closed end refers to a shield placed over both ends of the cylinder formed by the cold shape. The model further shows that any gap between the edges of each side of the facesheet where they meet over the flow tube in the cold shape has an influence on the maximum turndown. Figure 13 shows the turndown from a perfect cold shape, or 0 mm gap, to 15 mm (0.59 in) gap. These turndown values are calculated by varying the cold shape relative to a hot shape having a radius of curvature of 1 m. On the other hand, as seen in Figure 14, turndown is not strongly sensitive to a radius of curvature in the hot shape greater than ~0.1 m. The values for this figure are calculated by varying the hot shape with respect to a cold shape having no gap. Both relationships indicate that emphasis needs to be placed primarily upon cold shape deformation and bias spring stiffness in the next phase of design while the curvature of the high temperature shape is a fairly flexible design parameter.

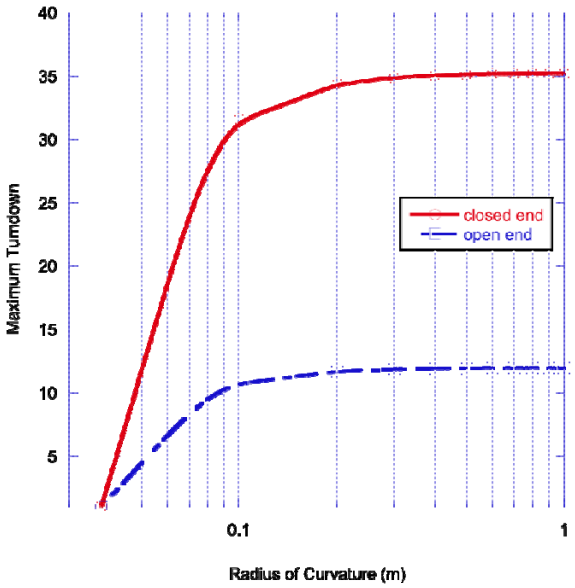

Figure 10 Sensitivity to curvature for the hot case. *Shows sensitivity in turndown to the hot case curvature of the facesheet. A curvature of 0.1 is approximately a half circle.*

Stress and deformation analysis shows that even after only a short (60 s) period of heating, the reconfigurable radiator panel can be seen to open substantially, with the majority of the flattening deformation induced by the SMA concentrated near the flow tube heat source. This can be seen in Figure 11. The contours in this figure show the axial stress in the glass fiber laminae transverse to the fiber direction, which corresponds to the largest stress component induced by the bending. The limits of the contour legend are equivalent to the calculated values for axial stresses at failure in this direction.

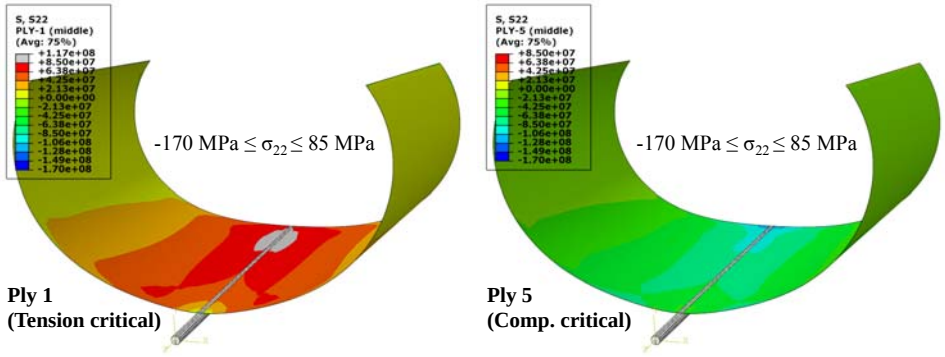

Figure 11 - Global heated deformation and local stress results (S22) in the glass fiber-based laminae (contour plot bounds correspond to stress limits).

Similar results can also be seen in Figure 12. The contours in this figure show the axial stress in the carbon fiber laminae aligned with the fiber direction, which corresponds to the largest stress component induced by the bending. As in the above, the limits of the contour legend are equivalent to the calculated values for axial stresses at failure in this fiber-aligned direction.

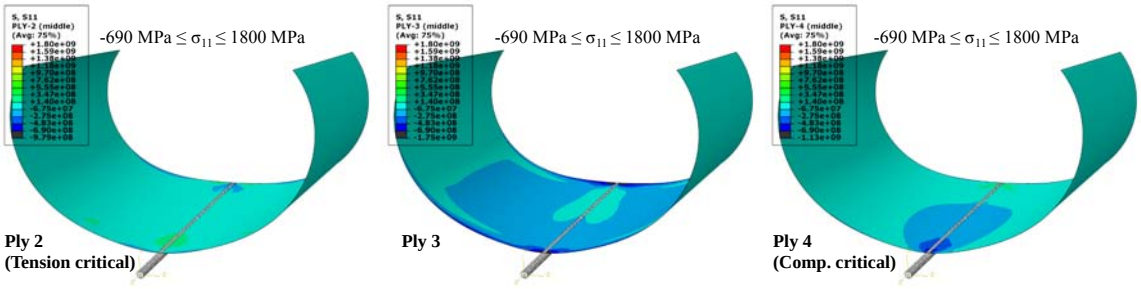

Figure 12 - Global heated deformation and local stress results (S11) in the carbon fiber-based laminae (contour plot bounds correspond to stress limits).

Benchtop Demonstration

Two benchtop demonstrations were performed to show proof of concept. The first was performed at Texas A&M using high temperature SMA material and heaters on a metal winglet structure in order to demonstrate the desired actuation. The second was performed at the Johnson Space Center using SMA with a transition temperature in the target range and on a scale composite based winglet structure.

The demonstrations are intended to:

- Reflect a single winglet section of the full scale thermal model at
  - Approximately half-scale at Texas A&M lab
  - Approximately full scale at JSC lab
- Demonstrate concept actuation under
  - Lab ambient conditions using heater induced temperature change

- Target application transition temperature using low temperature environment chamber.

- Be simple in configuration,
- Based on thermally induced transformation strains generated by commercially available (i.e., fully stabilized) SMA wire.

The Texas A&M demo was fabricated as schematically described in Figure 14. The basic structural material consisted of stainless steel foil (0.002 in thick) onto which a layer of thermal graphite sheet (0.004 in thick) was adhered for greatly increased thermal conductivity. The total planar dimensions of the two-ply laminate were 5 in long by 2 in wide. It was determined using preliminary finite element analysis that two 0.3 mm diameter wires recovering 4% (contractile) strain would have sufficient strength and deformation to morph the winglet as needed. The wires were installed in an "x" configuration as shown in Figure 14, the end of each wire terminating by passing through several small holes at the ends of the sheet, which provided sufficient friction to prevent wire slipping. A small droplet of super glue applied to each hole further secured the wire. After assembly, each sheet was rolled in the long direction to form an open circle section with a diameter of ~1.6 in.

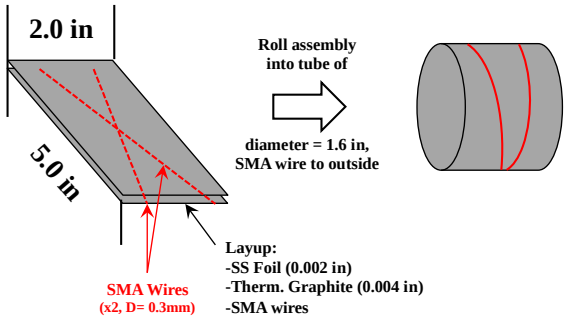

Figure 14 - A schematic showing the proof-of-concept morphing radiator winglet design

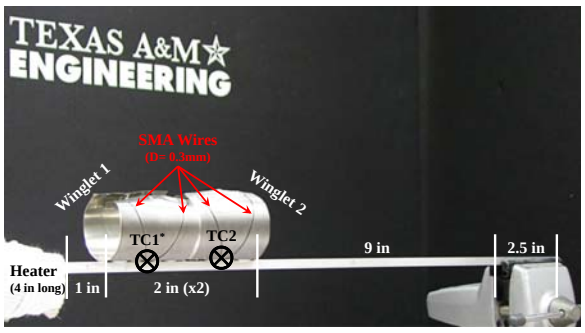

Figure 13 - Test setup for the morphing radiator winglet demonstration

The full thermal test assembly consisted of two morphing winglets attached to an aluminum rod with a square cross-section (0.25 in x 0.25 in), which itself was held by a bench vice at one end and was wrapped with resistive heating tape on the other. A thermocouple was inserted at the center of each of the two winglet/rod interfaces (see Figure 15), the first (left) one being used to control the heater output, and the second providing information on any disparities in temperatures between winglets 1 and 2. An IR camera (Testo 885-1 Thermal Imager) was used to qualitatively record both localized heating and global deformations.

The demonstration test stepped heater temperature from 50°C through 140°C in 10°C increments allowing winglet temperatures to stabilize at each increment. After 30 min at the peak temperature, the heater is removed and the system allowed to cool. The resulting winglet temperatures can be seen in Figure 22. Note the substantial disparity between the temperatures of the two winglets due to the effectiveness of the first in transferring heat energy out of the aluminum rod and into the ambient environment.

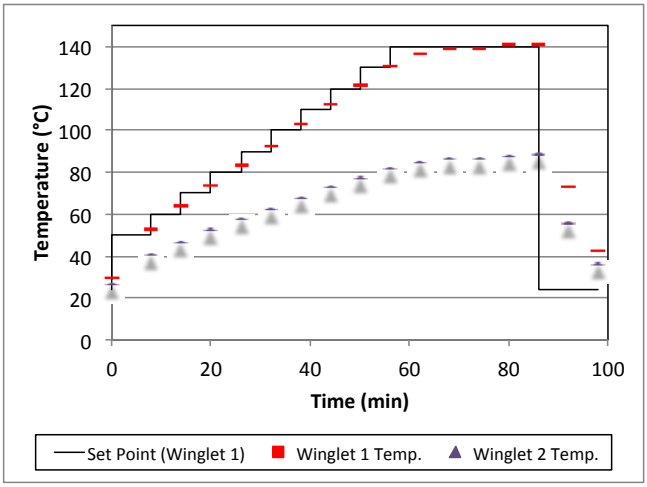

Figure 15 - Setpoint and measured temperatures on the morphing radiator demonstration

Though similar in many respects, the JSC demo differs from that performed at Texas A&M in that it is intended to show both the plausibility of the composite material for use in a flexible facesheet and actuation in the target application temperature range. The winglet is fabricated from a 5-ply composite layup similar to the concept design but with a somewhat larger cold shape diameter due to mold materials that were on hand to fabricate the unsprung shape. The shape memory wire used has a low transition temperature near freezing.

In this test the winglet and wire are soaked at below -20C during and following assembly. The assembled winglet is then removed from the low temperature environment chamber and placed on a table at room temperature. The sequence shown in Figure 24 depicts the actuation of the facesheet from below freezing to a nearly flat hot shape that spans 12 inches. Note the white areas on the facesheet indicating frost in the top frame. By the second frame most frost has melted but some remains until the final frame, whereupon most of the actuation has occurred.

The actuation observed in both tests is shown in during the controlled heating procedure successfully demonstrated that the self-morphing radiator of concept A was in fact feasible at the scale considered. Thermal and IR images at the initial and final state as well as at the 100°C and 140°C set points are shown in Figure 17, and images at all set points are available. It is clear that as the center of the first winglet reaches 100°C, noticeable thermally induced morphing has occurred, though the temperature of the second winglet is insufficient to induced actuation. However, as the first winglet reaches ~140°C and exhibits substantial deformation toward a flat (open) configuration, the second winglet has begun to open as well. Upon removal of the heater power, the system cools toward room temperature once again and the winglets begin to recover their initial shape.

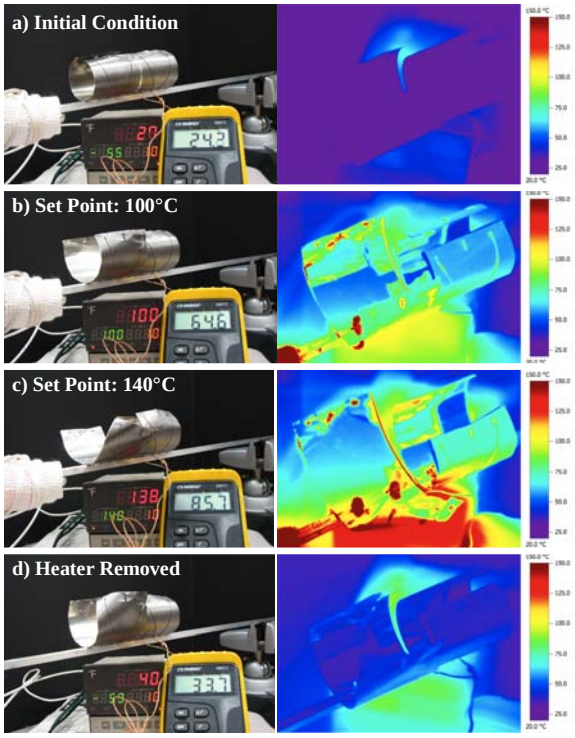

Figure 17 - A series of images showing the actuation of a proof-of-concept for the morphing radiator concept.

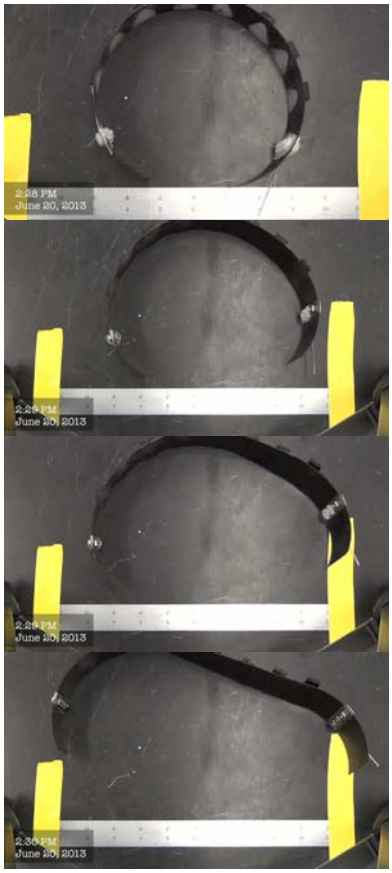

Figure 16 - low temperature with composite facesheet proof-of-concept demonstration

VI. Conclusions

A unique concept for high turndown thermal control of manned space vehicles that utilizes shape memory alloys has been explored through analysis and benchtop prototype testing. Results indicate that:

- High thermal control system turndown ratios of 35.2:1 are predicted in a likely mission scenario with a simple, single fluid-loop thermal control system.
- Physical turndown provided by the radiator can approach 96:1.
- Turndown capability is most sensitive to cold-shape geometry where gaps in the geometry raise the view factor of the radiating surface to space.
- Limited turndown sensitivity to hot shape affords flexibility in continued development of the technology
- The desired actuation behavior has been modeled and the concept shown capable of reproducing the range of actuation needed in response to fluid loop temperature variation alone.
- The desired actuation behavior has been reproduced in benchtop prototypes of the concept tested at Texas A&M University and at the NASA Johnson Space Center.

The strength of this technology is its entirely passive behavior in response to changing environment and vehicle heat loads. This behavior means that this

technology can produce very high turn-downs which enable single-loop thermal control without active control, power draw, or instrumentation. By enabling single loop thermal control, it also promises to reduce thermal control system launch mass by approximately 25%. For the Orion CEV this amounts to a projected mass reduction of between 139 kg and 225 kg.

VII. References

[1]Ochoa, D., Vonau, W., and Ewert, M., "A Comparison between One- and Two-Loop ATCS Architectures Proposed for CEV," SAE Int. J. Aerosp. 4(1):344-350, 2011, doi:10.4271/2009-01-2458

[2]Navarro, Moses, "Lunar Lander 1-Loop versus 2-Loop Active Thermal Control Trade Study," ESC Group, ESCG-4470-07-TEAN-DOC-0099, Delivered to NASA Aug 24, 2007

[23] JSC/ESCG guidance

[24] Donabedian, M., Gilmore, D., et.al, "Insulation," Spacecraft Thermal Control Handbook, Volume I: Fundamental Technologies, 2nd edition, edited by D. Gilmore, 2002, P165

[25] Rohsenow W.M., et al., Handbook of Heat Transfer, 3rd ed, McGraw-Hill, p. 7.84

[26] Incropera, F. & Dewitt, D. Fundamentals of heat and mass transfer, 5th edition. John Wiley and Sons, 2002. p. 794.

[27] Rohsenow W.M., et al., Handbook of Heat Transfer, 3rd ed, McGraw-Hill, p. 7.80.

[28] Thermal Desktop paper…

[33] D. Hartl, D. Lagoudas, F. Calkins, "Advanced Methods for the Analysis, Design, and Optimization of SMA-Based Aerostructures," Smart Materials and Structures, Vol. 20, 094006, 2011.

[34] D. Lagoudas, D. Hartl, Y. Chemisky, L. Machado, P. Popov, "Constitutive Model for Polycrystalline Shape Memory Alloys with Smooth Transformation Surfaces," International Journal of Plasticity, Vol. 32–33, pp. 155–183, 2012.

[35] D. Hartl, D. Lagoudas, "Constitutive Modeling and Structural Analysis Considering Simultaneous Phase Transformation and Plastic Yield in Shape Memory Alloys," Smart Materials and Structures, Vol. 18, No. 10 , 2009.

[36] Siegel and Howell, Thermal radiation heat transfer, 4th edition, p.843